Numerical Noise Analysis for Nonlinear Circuits with a Periodic Large Signal Excitation Including Cyclostationary Noise Sources

Makiko Okumura, Hiroshi Tanimoto, Tetsuro Itakura, and Tsutomu Sugawara, *Member, IEEE*

Abstract—**A numerical small signal noise analysis method for nonlinear circuits with a periodic large signal excitation, e.g., mixer circuits and switching circuits, is proposed. For small signal input responses, these nonlinear circuits are modeled as their linear periodic time-varying circuits. First, a numerical calculation method for the time-varying transfer function of a linear periodic time-varying circuit is described. Next, a noise analysis method is proposed for these circuits which contain noise sources modeled as cyclostationary random processes. Thermal noise and shot noise in the presence of periodic large signal excitation are modeled as cyclostationary random processes, each of which is modeled as a set of stationary random processes in continuous time. Aliasing components folded back to the baseband from high-frequency bands are calculated, and their powers are accumulated until their contributions become negligible. Simulated noise figures closely matched the measured values.**

I. Introduction

AMONG nonlinear circuits with multiple frequency excitations, there is a class of significant circuits with two excitations where one of the excitations is large and the other is small, e.g., switched capacitor networks, modulators, and frequency converters. This paper describes a numerical small signal noise analysis method for such nonlinear circuits which have a periodic large signal excitation.

There have been many papers published on analysis of the steady-state behavior of nonlinear circuits with multiple frequency excitations [1]–[5]. They can be applied to a wide range of nonlinear circuits; however, extensive computation is needed and they cannot treat noises. In contrast, small signal analysis for nonlinear circuits with a periodic large signal excitation can be expected to be much more efficient if the circuits are modeled as their linear periodically time-varying (LPTV) circuits for the small signals including noises. The LPTV circuit can be obtained as a first order Taylor expansion around a steady-state response. Hence, it is necessary first to find its steady-state response for the periodic large signal excitation.

There are two major techniques for finding the periodic steady-state response: the shooting method [6, 7] and the harmonic balance method [8]. A small signal analysis method for mixer circuits is described in [9] using the conversion matrix technique in the frequency domain based on the harmonic balance method. Although the Fourier components of the periodically time-varying transfer function are readily available in this type of small signal analysis, the computational cost becomes prohibitively large when the transfer function has large high order Fourier components. By using the shooting method, the authors proposed a small signal analysis method where the LPTV circuit model is obtained along with the steady-state analysis [10]. In this reference, however, it was not clearly described how to obtain the Fourier components of the periodically time-varying transfer function from the steady-state solution. The first contribution of this paper is to further develop the method to compute the time-varying transfer functions for the LPTV circuits described in [10].

Estimating the noise figures in LPTV circuits is a difficult problem because the estimation must take into account "aliasing" from higher frequency bands to the baseband, and because the statistical parameters of the nosie sources in the circuits vary with time. For example, the shot noise of a diode depends on its conducting current, which varies periodically due to the periodic large signal excitation. Therefore, the noise needs to be modeled by a cyclostationary random process [11].

Noise analysis methods for switched capacitor networks (SCNs) [12]–[18] have been proposed which assume that the noise sources are stationary random processes. For example, exact noise analysis for SCNs has been reported [17], [18]. The authors also have proposed a noie analysis method for LPTV circuits like frequency converters [19], [20]. However, all these methods cannot handle noise sources in nonlinear elements which are excited by a large signal excitation, i.e., cyclostationary noises. The second contribution of this paper is to extend the algorithm to

Manuscript received January 10, 1992; revised January 5, 1993. This paper was recommended by Associate Editor J. A. Nossek.

The authors are with the Research and Development Center, Toshiba Corporation, 1, Komukai Toshiba-cho, Saiwai-ku, Kawasaki 210, Japan.

IEEE Log Number 9210963.

1057-7122/93$03.00

numerical noise analysis for LPTV circuits including noise sources modeled by cyclostationary random processes.

These methods can be classified as a generalized analysis method for LPTV circuits [21]. These algorithms have been implemented in a circuit simulator SPREAD [22], which is an in-house simulator based on SPICE2 [23].

In Section II, the numerical small signal analysis method is revisted and reorganized to obtain a small signal LPTV equivalent circuit. In Section III, a modeling of cyclostationary noises is introduced, and a noise analysis including cyclostationary noises is presented. An exact noise solution for a simple switching circuit is compared with the simulation result in the section. Some practical examples are shown in Section IV, including switched capacitor circuits and a direct conversion mixer circuit. Good agreement with measured data supports the proposed algorithm.

II. Small Signal Analysis Method

A. Linear Periodically Time-Varying Circuit

Nonlinear circuits with a periodic large signal excitation are modeled as LPTV circuits for a small signal response. An equivalent LPTV circuit is derived by linearizing the nonlinear circuit around the periodic steady-state response in the time domain.

Consider a system with a periodic large signal excitation $\boldsymbol{v}(t)$ and a small signal $\delta\boldsymbol{v}(t)$:

$$\boldsymbol{f}(\boldsymbol{y}(t), \dot{\boldsymbol{y}}(t)) = \boldsymbol{v}(t) + \delta\boldsymbol{v}(t), \tag{1}$$

where $\boldsymbol{v}(t)$ is a T-periodic excitation with respect to time t, $\boldsymbol{y}(t)$ and $\boldsymbol{v}(t)$ are N_s dimensional vectors, and $\dot{\boldsymbol{y}}(t)$ denotes the time derivative of $\boldsymbol{y}(t)$. Assume that system (1) has a stable periodic solution $\boldsymbol{y}_{st}(t)$ with period T; that is, $\boldsymbol{y}_{st}(t+T) = \boldsymbol{y}_{st}(t)$ for all t values. It is also assumed that $\boldsymbol{f}$ is differentiable with respect to $\boldsymbol{y}$ and $\dot{\boldsymbol{y}}$ for $\boldsymbol{y}_{st}(t)$.

Consider the first order expansion of the left-hand side of (1) around the periodic steady-state response $\boldsymbol{y}_{st}(t)$ to linearize the nonlinear periodic circuit:

$$\boldsymbol{f}(\boldsymbol{y}_{st}(t), \dot{\boldsymbol{y}}_{st}(t)) + \frac{\partial \boldsymbol{f}}{\partial \boldsymbol{y}}\,\delta\boldsymbol{y}(t) + \frac{\partial \boldsymbol{f}}{\partial \dot{\boldsymbol{y}}}\,\delta\dot{\boldsymbol{y}}(t) \approx \boldsymbol{v}(t) + \delta\boldsymbol{v}(t). \tag{2}$$

The above equation can be rewritten as

$$\boldsymbol{g}(t)\boldsymbol{x}(t) + \boldsymbol{c}(t)\dot{\boldsymbol{x}}(t) = \boldsymbol{u}(t), \tag{3}$$

where

$$\boldsymbol{x}(t) \equiv \delta\boldsymbol{y}(t), \quad \dot{\boldsymbol{x}}(t) \equiv \delta\dot{\boldsymbol{y}}(t), \quad \boldsymbol{u}(t) \equiv \delta\boldsymbol{v}(t),$$

$$\boldsymbol{g}(t) \equiv \left.\frac{\partial \boldsymbol{f}}{\partial \boldsymbol{y}}\right|_{\boldsymbol{y}(t)=\boldsymbol{y}_{st}(t)}, \quad \boldsymbol{c}(t) \equiv \left.\frac{\partial \boldsymbol{f}}{\partial \dot{\boldsymbol{y}}}\right|_{\dot{\boldsymbol{y}}(t)=\dot{\boldsymbol{y}}_{st}(t)}.$$

Note that $\boldsymbol{g}(t)$ and $\boldsymbol{c}(t)$ are T-periodic, i.e., $\boldsymbol{g}(t+T) = \boldsymbol{g}(t)$ and $\boldsymbol{c}(t+T) = \boldsymbol{c}(t)$. System (3) is an LPTV circuit.

B. Small Signal Steady-State Solution

The small signal steady-state response $\boldsymbol{x}_{st}(t)$ for system (3) can be written using the time-varying transfer function [21]

$$\boldsymbol{x}_{st}(t) = \frac{1}{2\pi}\int_{-\infty}^{\infty} \boldsymbol{H}(j\Omega, t)\boldsymbol{U}(j\Omega)e^{j\Omega t}\,d\Omega, \tag{4}$$

where $\boldsymbol{H}(j\Omega, t)$ is the time-varying transfer function and forms an $N_s \times N_s$ matrix. $\boldsymbol{U}(j\Omega)$ is the Fourier transform of the input signal and is an N_s dimensional vector.

Let the input for system (3) be

$$\boldsymbol{u}(t) = \boldsymbol{u}e^{j\omega_I t}, \tag{5}$$

where ω_I is the input frequency and the $\boldsymbol{u}$ vector generally indicates the magnitudes of the input signals, but here, $\boldsymbol{u}$ is a normalized vector for convenience. For example, when only one source is connected to the $\boldsymbol{k}$th state, the $\boldsymbol{k}$th element of $\boldsymbol{u}$ is "1" and the remaining elements are "0". Substituting the Fourier transform of (5) into (4), the small signal steady-state response $\boldsymbol{x}_{st}(t)$ can be written as

$$\boldsymbol{x}_{st}(t) = \boldsymbol{H}(j\omega_I, t)\boldsymbol{u}e^{j\omega_I t}. \tag{6}$$

The time-varying transfer function is also T-periodic [24] and can be represented using the Fourier series, since system (3) is periodic. The Fourier coefficients are written by

$$\boldsymbol{H}_l(j\omega_I) = \frac{1}{T}\int_0^T \boldsymbol{H}(j\omega_I, t)e^{-jl\omega_s t}\,dt, \tag{7}$$

where $\omega_s \equiv 2\pi/T$. $\boldsymbol{H}_l(j\omega_I)$ can be interpreted as the transfer function for the output response with a frequency of $\omega_I + l\omega_s$.

C. Numerical Calculation of the Time-Varying Transfer Function

In this section, $\boldsymbol{H}_l(j\omega_I)$ is calculated numerically. First, divide the period T into p intervals, and $\boldsymbol{H}(j\omega_I)$ is represented using a time-sampled version of $\boldsymbol{H}(j\omega_I, t)$.

The variables are defined by the equations

$$T = \sum_{m=1}^{p} h_m, \qquad \tau_m = \sum_{k=1}^{m} h_k.$$

Therefore, $\tau_p = T$ and $\tau_0 = 0$ is introduced for convenience. Here, it is assumed that $\boldsymbol{H}(j\omega_I, t)$ is time-invariant within each interval $\tau_{m-1} < t \le \tau_m$ for $m = 1, 2, \ldots, p$. Then the integration of (7) can be replaced by a summation

$$\boldsymbol{H}_l(j\omega_I) = \sum_{m=1}^{p} \boldsymbol{H}(j\omega_I, \tau_m)K_m^l, \tag{8}$$

where $\boldsymbol{H}(j\omega_I, \tau_m)$ is a time-sampled version of $\boldsymbol{H}(j\omega_I, t)$ at $t = \tau_m$, K_m^l is defined by

$$K_m^l \equiv \frac{h_m}{T}\,\mathrm{Sa}\left(\frac{l\omega_s h_m}{2}\right)e^{-jl\omega_s(\tau_{m-1}+h_m/2)}, \tag{9}$$

where $\mathrm{Sa}(\cdot)$ is a sampling function defined by

$$\mathrm{Sa}(x) \equiv \frac{\sin(x)}{x}.$$

Next, consider how to compute the time-sampled version of the time-varying transfer function, $\boldsymbol{H}(j\omega_l, \tau_m)$, in (8). An approximate solution of $\boldsymbol{H}(j\omega_l, \tau_m)$ is computed using (3) and (6) at discrete times. The differential equation of (3) is approximated by numerical integration.

Substituting (5) and discrete times, $nT + \tau_m$, into (3), the small signal steady-state response $\boldsymbol{x}_{\mathrm{st}}(t)$ must satisfy the following equation at discrete time points:

$$\boldsymbol{g}(nT + \tau_m)\boldsymbol{x}_{\mathrm{st}}(nT + \tau_m) + \boldsymbol{c}(nT + \tau_m)\dot{\boldsymbol{x}}_{\mathrm{st}}(nT + \tau_m) = \boldsymbol{u}e^{j\omega_l(nT+\tau_m)} \quad \text{for } m = 1, 2, \ldots, p. \tag{10}$$

Since $\boldsymbol{g}$ and $\boldsymbol{c}$ are periodic, $\boldsymbol{g}(nT + \tau_m) = \boldsymbol{g}(\tau_m) \equiv \boldsymbol{g}_m$ and $\boldsymbol{c}(nT + \tau_m) = \boldsymbol{c}(\tau_m) \equiv \boldsymbol{c}_m$. Equation (10) can be rewritten as

$$\boldsymbol{g}_m\boldsymbol{x}_{\mathrm{st}}(nT + \tau_m) + \boldsymbol{c}_m\dot{\boldsymbol{x}}_{\mathrm{st}}(nT + \tau_m) = \boldsymbol{u}e^{j\omega_l(nT+\tau_m)}. \tag{11}$$

The differential equation (11) is approximately solved using numerical integration. Applying the backward Euler method, for example, we have

$$\left(\boldsymbol{g}_m + \frac{\boldsymbol{c}_m}{h_m}\right)\hat{\boldsymbol{x}}_{\mathrm{st}}(nT + \tau_m) - \frac{\boldsymbol{c}_m}{h_m}\hat{\boldsymbol{x}}_{\mathrm{st}}(nT + \tau_{m-1}) = \boldsymbol{u}e^{j\omega_l(nT+\tau_m)} \quad \text{for } m = 1, 2, \ldots, p, \tag{12}$$

where the caret ($\hat{}$) means an approximate solution. The error for the numerical integration will be discussed later. By definition of (6), the relationship between $\hat{\boldsymbol{H}}(j\omega_l, \tau_m)$ and $\hat{\boldsymbol{x}}_{\mathrm{st}}(nT + \tau_{m-1})$ can be written as

$$\hat{\boldsymbol{x}}_{\mathrm{st}}(nT + \tau_m) = \hat{\boldsymbol{H}}(j\omega_l, \tau_m)\boldsymbol{u}e^{j\omega_l(nT+\tau_m)}. \tag{13}$$

Substituting (13) into (12) gives

$$\left(\boldsymbol{g}_m + \frac{\boldsymbol{c}_m}{h_m}\right)\hat{\boldsymbol{H}}(j\omega_l, \tau_m)\boldsymbol{u} - \frac{\boldsymbol{c}_m}{h_m}\hat{\boldsymbol{H}}(j\omega_l, \tau_{m-1})\boldsymbol{u}e^{-j\omega_l h_m} = \boldsymbol{u} \quad \text{for } m = 1, 2, \ldots, p. \tag{14}$$

Since the transfer function is periodic,

$$\hat{\boldsymbol{H}}(j\omega_l, \tau_0) = \hat{\boldsymbol{H}}(j\omega_l, \tau_p). \tag{15}$$

Rearranging (14) and (15) into matrix form, we have

$$\underbrace{\begin{bmatrix} \boldsymbol{J}_1 & & & \boldsymbol{C}_1 \\ \boldsymbol{C}_2 & \boldsymbol{J}_2 & & \\ & \ddots & \ddots & \\ & & \boldsymbol{C}_p & \boldsymbol{J}_p \end{bmatrix}}_{\equiv \boldsymbol{T}} \cdot \begin{bmatrix} \hat{\boldsymbol{X}}_1 \\ \hat{\boldsymbol{X}}_2 \\ \vdots \\ \hat{\boldsymbol{X}}_p \end{bmatrix} = \begin{bmatrix} \boldsymbol{u} \\ \boldsymbol{u} \\ \vdots \\ \boldsymbol{u} \end{bmatrix}, \tag{16}$$

where

$$\hat{\boldsymbol{X}}_m \equiv \hat{\boldsymbol{X}}(j\omega_l, \tau_m) \equiv \hat{\boldsymbol{H}}(j\omega_l, \tau_m)\boldsymbol{u},$$

$$\boldsymbol{J}_m \equiv \boldsymbol{g}_m + \frac{\boldsymbol{c}_m}{h_m}, \qquad \boldsymbol{C}_m \equiv -e^{-j\omega_l h_m}\frac{\boldsymbol{c}_m}{h_m}.$$

$\hat{\boldsymbol{X}}_m$ is a column vector of $\hat{\boldsymbol{H}}(j\omega_l, \tau_m)$, which is selected by the $\boldsymbol{u}$ vector, where $\boldsymbol{u}$ is as described previously.

Block matrices $\boldsymbol{J}_m$ and $\boldsymbol{C}_m$ can be obtained using a general-purpose circuit simulator. The discretization step h_m is the numerical integration time step in the transient analysis for the periodic steady-state response. The periodic response is calculated using the shooting method [7] in SPREAD. Note that each $\boldsymbol{J}_m$ matrix in the system of (16) exists in an LU factorized form, with a sparse matrix pointer system at each integration time point.

Finally, the Fourier components, $\boldsymbol{H}_l(j\omega_l)$, are computed by

$$\boldsymbol{H}_l(j\omega_l)\boldsymbol{u} = \sum_{m=1}^{p} \hat{\boldsymbol{X}}_m K_m^l. \tag{17}$$

Figure 1 is a graphical representation of the calculation for the time-varying transfer function. An inverse matrix of the large matrix $\boldsymbol{T}$ in (16) represents the operator $\mathcal{T}(\omega_l)$ in Fig. 1.

D. Errors in the Algorithm

Errors of the time-varying transfer function in this algorithm arise in the discretization of (8) and the numerical integration of (12). First, the error for the numerical integration is discussed.

The error, ϵ_l, is defined by

$$\epsilon_l \equiv H(j\omega, \tau_i) - \hat{H}(j\omega, \tau_i),$$

where $H(j\omega, \tau_i)$ is an exact solution and $\hat{H}(j\omega, \tau_i)$ is an approximate solution. From (6) and (13), the error ϵ_l can be written as

$$\epsilon_l = [x_{\mathrm{st}}(nT + \tau_i) - \hat{x}_{\mathrm{st}}(nT + \tau_i)]e^{-j\omega(nT+\tau_i)}.$$

The error magnitude of $\hat{H}(j\omega, \tau_i)$ is the same as that of $\hat{x}_{\mathrm{st}}(j\omega, \tau_i)$ for the numerical integration, since $|e^{j\omega t}| = 1$. The local truncation errors in numerical integrations have been discussed in pertinent literature [25]. The trade-offs among the steps, orders of the numerical integration, and the computational cost are well known. Application of the algorithm for the small signal analysis method to high-order numerical integrations and the frequency warping effects in numerical integrations are described in [22].

Discretization of this algorithm requires the input frequencies to be lower than the equivalent "Nyquist" frequency $\omega_{\max}$:

$$\omega_{\max} = \frac{\pi}{h_{\max}}, \tag{18}$$

where $h_{\max}$ is the maximum value of the numerical integration time step h_m ($m = 1, 2, \ldots, p$). The smaller the time step used for discretization in this algorithm, the higher the frequency components that can be computed.

III. Noise Analysis Method

A. Cyclostationary Random Process

The noise sources for LPTV circuits contain random signals which must be modeled by cyclostationary random

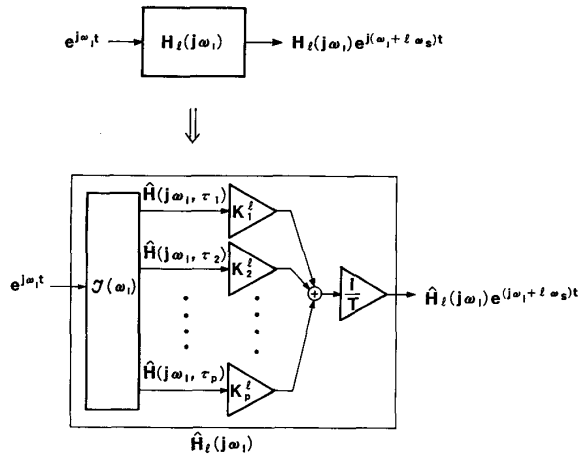

Fig. 1. Calculation of $\hat{H}(\omega_\ell)$. This is a graphical representation of (10). Discrete transfer functions are calculated by the operator $\mathcal{T}(\omega_\ell)$.

processes in addition to stationary random processes. The thermal noise density of a resistor R can be expressed as $v_{\text{thermal}} = \sqrt{2kTR}$. In this expression, R may change with a periodic large signal excitation; for example, the ON resistance of an MOS transistor changes with excitation. The shot noise current density of a diode conducting current I_d can be expressed as $i_{\text{shot}} = \sqrt{qI_d}$. Again, this noise current may change with a periodic large signal excitation through a change in I_d. If the mechanisms for these noises are not affected by the periodic excitation and the change can be seen to be sufficiently slow compared with the noise generating mechanisms, these noise sources can be modeled as slowly amplitude modulated white noises, and thus modeled as cyclostationary random processes. Then, the noise modeled is no longer white. As used in this paper, "cyclostationary" means cyclostationary in the wide sense; the modifier *wide sense* is omitted.

Thermal noise and shot noise are modeled as a set of randomly occurring impulses. These impulses are consequences of the random motion of free electrons by thermal agitation for thermal noise. A change in the operating point will not affect the noise generating mechanism in this case. The impulses are caused by random emission and the motion of carriers in the shot noise case. It is well recognized that experimental results support the validity of the shot noise formula for a very wide range of operating currents. Since the bandwidth of thermal noise is about 6×10^{12} Hz at room temperature [26], and the bandwidth of shot noise is typically in the high gigahertz range [11], time samples of thermal noise and shot noise that are discretized by more than several tens of picoseconds can be regarded as uncorrelated samples. Hence, this led us to the above-mentioned model of the slowly amplitude modulated white noise, which can be considered as a mean square periodicity process [27].

B. Modeling of the Cyclostationary Random Process

The characterization of cyclostationary processes has been described in [28]–[31]. Several methods for representing a cyclostationary process in terms of joint stationary processes have been developed [29]. In this paper, cyclostationary noise is modeled by a set of independent stationary noises in continuous time, because this makes it possible to use conventional noise analysis methods.

In this paper, a cyclostationary random signal is modeled as shown in Fig. 2. The number of numerical integration time points in one period is used for the number of discrete points, as explained in Section II. In Fig. 2, it is five for convenience. Assuming that the individual noise sources are stationary while $\tau_{m-1} < t \le \tau_m$, $m = 1, 2, \ldots, p$, because $\boldsymbol{H}(j\omega, t)$ is time-invariant during individual intervals, the noise signal can be modeled by a stationary process during the interval. It can also be assumed that the stationary processes for individual intervals are uncorrelated from the discussion in the previous subsection. Therefore, an individual random signal is modeled as a hypothetical stationary process multiplied by one of the periodic window functions which have different time delays, different widths, and are nonoverlapping. The individual stationary random processes are represented using the Fourier series [32]. The equivalent noise values for circuit simulation are then computed from the power spectral densities of the random processes. Therefore, a numerical noise analysis for the circuits in which the noise sources are modeled by cyclostationary random processes becomes possible using a general circuit simulator.

The cyclostationary process $c(t)$ modeled, as shown in Fig. 2, is represented by

$$c(t) = \sum_{m=1}^{p} n_m(t) w_m(t), \tag{19}$$

where $n_m(t)$ is a stationary random signal and $w_m(t)$ is a window function for the mth interval.

The window function in (19) is T-periodic with a width of h_m and is given by

$$w_m(t) = r_m(t) \otimes \sum_{n=-\infty}^{\infty} \delta(t - nT) \quad \text{for } m = 1, 2, \ldots, p,$$

where

$$r_m(t) = \begin{cases} 1 & \text{for } \tau_{m-1} < t \le \tau_m, \\ 0 & \text{otherwise,} \end{cases}$$

and the symbol $\otimes$ represents a convolution. They are nonoverlapping with differing time delays.

An individual stationary random signal can be represented by a formal Fourier series

$$n_m(t) = \sum_{\mu=-\infty}^{\infty} A_{m\mu} e^{j\mu(2\pi/c)t}, \tag{20}$$

where $A_{m\mu}$ is a random variable with the following properties:

$$E[A_{m\mu}] = 0$$

$$E\left[A_{m\mu}^2\right] = \frac{1}{2\pi} S_m(\omega_\mu)\, \Delta\omega \tag{21}$$

$$E[A_{ml} A_{mk}] = 0, \qquad l \ne k, \text{ for } m = 1, 2, \ldots, p. \tag{22}$$

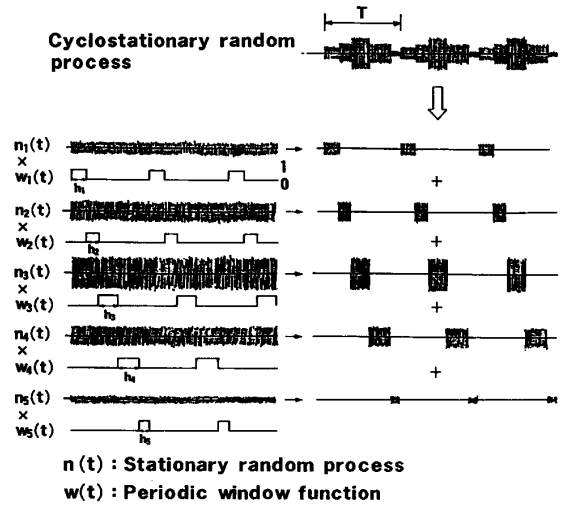

Fig. 2. Model of a cyclostationary random process. Individual stationary random signals may have different power spectral densities. Periodic window functions are T-periodic with a width of h_m. The window functions are nonoverlapping with differing time delays.

From the above assumption,

$$E[A_{l\mu}A_{k\mu}] = 0, \qquad l \neq k, \text{ for } l,k = 1,2,\ldots,p, \quad (23)$$

where

$$\Delta\omega = \frac{2\pi}{c},$$
$$\omega_\mu = \mu\Delta\omega.$$

$E[\cdot]$ indicates the ensemble average.

The cyclostationary thermal and shot noises are modeled in this way. Flicker noise generated under a periodic large signal excitation cannot be modeled as a cyclostationary process by using this method, because it has very long time constants and thus equation (23) does not hold. However, flicker noises may exist as independent noise sources which are practically modeled as stationary random processes.

Substituting the Fourier transform of (19) into (4), the output noise signal is obtained by

$$y(t) = \sum_{n=-\infty}^{\infty}\sum_{\mu=-\infty}^{\infty} \boldsymbol{H}(\omega_\mu + n\omega_s, t) \cdot \sum_{m=1}^{p} A_{m\mu}R_{m,n}e^{j(\omega_\mu+n\omega_s)t}\boldsymbol{v},$$

where $\boldsymbol{v}$ is a normalized vector which indicates the noise source location the same as the $\boldsymbol{u}$ vector and

$$R_{m,n} \equiv \frac{h_m}{T}\,\mathrm{Sa}\left(\frac{n\omega_s h_m}{2}\right)e^{-jn\omega_s(\tau_{m-1}+h_m/2)}.$$

The instantaneous probabilistic spectral density matrix, denoted by $\boldsymbol{S}(\Omega,t)$, is the Fourier transform of the instantaneous probabilistic autocorrelation [11]

$$\boldsymbol{S}(\Omega,t) \equiv \int_{-\infty}^{\infty}\boldsymbol{R}_{yy}\left(t+\frac{\tau}{2},t-\frac{\tau}{2}\right)e^{-j\Omega\tau}d\tau, \quad (24)$$

where

$$\boldsymbol{R}_{yy} \equiv E\left[\boldsymbol{y}\left(t+\frac{\tau}{2}\right)\boldsymbol{y}^*\left(t-\frac{\tau}{2}\right)\right]$$

and where $\boldsymbol{S}(\Omega,t)$ and $\boldsymbol{R}_{yy}(t+\tau/2, t-\tau/2)$ are $N_s \times N_s$ dimensional matrices and the asterisk (*) indicates transposition and conjugation. Using (21), (22), and (23) and expanding the time-varying transfer functions by a Fourier series,

$$\boldsymbol{R}_{yy}\left(t+\frac{\tau}{2},t-\frac{\tau}{2}\right) = \frac{1}{2\pi}\sum_{\mu=-\infty}^{\infty}\sum_{n=-\infty}^{\infty}\sum_{r=-\infty}^{\infty}\sum_{l=-\infty}^{\infty}\sum_{q=-\infty}^{\infty} \cdot \boldsymbol{H}_l(\omega_\mu+n\omega_s)\boldsymbol{v}\boldsymbol{v}^*\boldsymbol{H}_q^*(\omega_\mu+r\omega_s) \cdot \sum_{m=1}^{p}R_{m,n}R_{m,r}^*S_m(\omega_\mu) \cdot e^{j(n-r+l-q)\omega_s t}e^{j\{\omega_\mu+(n+k+l+q)\omega_s/2\}\tau}\Delta\omega. \quad (25)$$

Substituting (25) into (24) and considering the limiting case $c \to \infty$ in (20), we obtain

$$\boldsymbol{S}(\Omega,t) = \int_{-\infty}^{\infty}\sum_{n=-\infty}^{\infty}\sum_{r=-\infty}^{\infty}\sum_{l=-\infty}^{\infty}\sum_{q=-\infty}^{\infty} \cdot \boldsymbol{H}_l(\omega+n\omega_s)\boldsymbol{v}\boldsymbol{v}^*\boldsymbol{H}_q^*(\omega+r\omega_s) \cdot \sum_{m=1}^{p}R_{m,n}R_{m,r}^*S_m(\omega)e^{j(n-r+l-q)\omega_s t} \cdot \delta\left\{\Omega-\omega-(n+r+l+q)\frac{1}{2}\omega_s\right\}d\omega. \quad (26)$$

The quantity $\boldsymbol{S}(\Omega,t)$ is referred to as the time-variant probabilistic spectral density. The spectral density which is actually measured is the time average of the time-variant probabilistic spectral density [11]. The time-averaged power spectral density matrix is given by

$$\langle \boldsymbol{S}(\Omega,t)\rangle = \int_{-\infty}^{\infty}\sum_{n=-\infty}^{\infty}\sum_{l=-\infty}^{\infty}\sum_{q=-\infty}^{\infty} \boldsymbol{H}_l\{\omega+n\omega_s\}\boldsymbol{v}\boldsymbol{v}^* \cdot \boldsymbol{H}_q^*\{\omega+(n+l-q)\omega_s\} \cdot \sum_{m=1}^{p}R_{m,n}R_{m,n+l-q}^*S_m(\omega) \cdot \delta\{\Omega-\omega-(n+l)\omega_s\}\,d\omega, \quad (27)$$

where $\langle\cdot\rangle$ is the time average. The power spectral density, aliased into the frequency of interest, ω_o, is calcu-

lated by

$$\boldsymbol{S}_{\text{alias}}(\omega_o) = \sum_{n=-\infty}^{\infty} \sum_{l=-\infty}^{\infty} \sum_{q=-\infty}^{\infty} \boldsymbol{H}_l(\omega_o - l\omega_s)\boldsymbol{v}\boldsymbol{v}^* \cdot \boldsymbol{H}_q^*(\omega_o - q\omega_s) \sum_{m=1}^{p} R_{m,n}R_{m,n+l-q}^* S_m\{\omega_o - (n+l)\omega_s\}. \tag{28}$$

Since the individual stationary random signal $n_m(t)$ in (20) is white noise as described in the previous subsection, the power spectrum $S_m(\omega)$ of $n_m(t)$ is constant. Then, the above equation can be resolved as follows:

$$\begin{aligned}\boldsymbol{S}_{\text{alias}}(\omega_o) = \sum_{n=-\infty}^{\infty} \Bigg[& \sum_{l=-\infty(l=q)}^{\infty} \boldsymbol{H}_l(\omega_o - l\omega_s)\boldsymbol{v}\boldsymbol{v}^* \cdot \boldsymbol{H}_l^*(\omega_o - l\omega_s) \sum_{m=1}^{p} |R_{m,n}|^2 S_m \\ & + \sum_{l=-\infty}^{\infty} \sum_{q=-\infty(l>q)}^{\infty} \boldsymbol{H}_l(\omega_o - l\omega_s)\boldsymbol{v}\boldsymbol{v}^* \cdot \boldsymbol{H}_q^*(\omega_o - q\omega_s) \sum_{m=1}^{p} R_{m,n}R_{m,n+l-q}^* S_m \\ & + \sum_{l=-\infty}^{\infty} \sum_{q=-\infty(l<q)}^{\infty} \boldsymbol{H}_l(\omega_o - l\omega_s)\boldsymbol{v}\boldsymbol{v}^* \cdot \boldsymbol{H}_q^*(\omega_o - q\omega_s) \sum_{m=1}^{p} R_{m,n}R_{m,n+l-q}^* S_m \Bigg] \end{aligned} \tag{29}$$

The imaginary part of the second and the third terms in (29) are cancelled, since they are conjugated with each other:

$$\begin{aligned}S_{\text{alias}}(\omega_o) = \sum_{n=-\infty}^{\infty} \Bigg[& \sum_{l=-\infty}^{\infty} \boldsymbol{H}_l(\omega_o - l\omega_s)vv^* \cdot H_l^*(\omega_o - l\omega_s) \sum_{m=1}^{p} |R_{m,n}|^2 S_m + 2\,\text{Real} \\ & \cdot \Bigg\{ \sum_{l=-\infty}^{\infty} \sum_{q=-\infty(l>q)}^{\infty} \boldsymbol{H}_l(\omega_o - l\omega_s)\boldsymbol{v}\boldsymbol{v}^* \cdot \boldsymbol{H}_q^*(\omega_o - q\omega_s) \sum_{m=1}^{p} R_{m,n}R_{m,n+l-q}^* S_m \Bigg\} \Bigg]. \end{aligned} \tag{30}$$

The autopower spectral density vector is the diagonal of (30). The approximate solution using truncated numbers N and L is written by

$$\begin{aligned}\boldsymbol{S}_{\text{alias}}(\omega_o) \approx \sum_{n=-N}^{N} \Bigg[& \sum_{l=-L}^{L} |\boldsymbol{H}_l(\omega_o - l\omega_s)\boldsymbol{v}|^2 \sum_{m=1}^{p} |R_{m,n}|^2 S_m \\ & + 2\,\text{Real} \Bigg\{ \sum_{l=-L}^{L} \sum_{q=-L(l>q)}^{L} \boldsymbol{H}_l(\omega_o - l\omega_s)\boldsymbol{v}\boldsymbol{v}^* \cdot \boldsymbol{H}_q^*(\omega_o - q\omega_s) \sum_{m=1}^{p} R_{m,n}R_{m,n+l-q}^* S_m \Bigg\} \Bigg]. \end{aligned} \tag{31}$$

The maximum value for N and L is limited by (18) in this method. Because the maximum frequency related to the input signal frequency ω_o which appears in the circuit is $|\omega_o + L\omega_s|$, L must satisfy the relation

$$|\omega_o + L\omega_s| \le \omega_{\max}.$$

This is true for N. Thus, the maximum value for N and L is given by the next inequality:

$$N, L \le \frac{\omega_{\max} - \omega_o}{\omega_s}. \tag{32}$$

Finally, consider a stationary random signal, a special case of this model. Since stationary random signals corresponding to each interval have the same spectral density value, their summation becomes one stationary random signal through a window function, whose width is T (i.e., $p = 1$). Then, the $\text{Sa}(\cdot)$ function is zero except for $n = 0$ and $n + l - q = 0$. Let $n = 0$ and $l = q$ in (28), and use truncated number L as the above case, and obtain

$$\boldsymbol{S}_{\text{alias}}(\omega_o) = \sum_{l=-L}^{L} \left| \boldsymbol{H}_l(\omega_o - l\omega_s)\boldsymbol{v}\sqrt{S(\omega_o - l\omega_s)} \right|^2. \tag{33}$$

This equation is exactly the same as that derived for a stationary noise [14].

This modeling for the cyclostationary noises does not assume any particular steady-state finding algorithm. The specific information required for noise calculation are h_m, S_m, and $\boldsymbol{H}_l(\cdot)$. Once h_m is determined, S_m can be obtained by the method described in this subsection. For the Fourier components $\boldsymbol{H}_l(\cdot)$, they are directly obtained by the harmonic balance method, while they are obtained via $\boldsymbol{J}_m$ and $\boldsymbol{C}_m$ matrices as by-products of the final transient analysis in the shooting method, as described in Section II.C.

C. Noise Sources

It is assumed that noise sources are uncorrelated and are considered as independent equivalent current sources. The noise sources allowed in the proposed method are shown in Table I.

As a flicker noise is not stationary [33], the above modeling technique cannot be applied to the flicker noise component generated under a periodic large signal excitation. However, the flicker noise contribution can be calculated practically if it is connected as an independent noise source, as is often modeled in the noise analysis for SC circuits [15]. In such cases, the flicker noise is approximately modeled as a linearly filtered stationary noise [33]. White noise and flicker noise are considered as independent stationary noise sources, while other noise sources are modeled as cyclostationary noises, as summarized in Table I.

D. Implementation of the Noise Analysis Algorithm

Since this paper employs the shooting method for finding the steady-state response, practical implementation is illustrated for that case.

TABLE I

Element	Kind of noise
(a) Stationary noise sources	
Resistor	Thermal noise
(Flicker noise)	—
(b) Cyclostationary noise sources	
Time-varying conductance	Thermal noise
Diode	Shot noise
Bipolar transistor	Shot noise
Junction FET	Channel conductance noise
MOSFET	Channel conductance noise

The equivalent current sources are connected in parallel with each noise source. The circuit equation to compute the transfer function X_k from the kth noise source is

$$TX_k = V_k, \qquad k = 1,2,\ldots,M,$$

where T is the large matrix on the left-hand side in (16), which is an $(N_s \times p)^2$ matrix. X_k and V_k are $N_s \times p$ vectors, and M is the number of noise sources in the circuit. V_k is defined by

$$V_k^t = (v_k^t, v_k^t, \ldots, v_k^t),$$

where v_k is an N_s vector which indicates the place of the kth nosie source, and t stands for transposition. Since $H_{k,l}$ and $H_{k,q}$ for l and q in (31) are calculated by using (17), the output equation is given by

$$\phi_{k,n,l,q} = (d_l^t X_k)(X_k^* d_q) B_{k,n,l,q}, \tag{34}$$

$$B_{k,n,l,q} = \sum_{m=1}^{p} R_{m,n} R_{m,n+l-q}^* S_{k,m}, \tag{35}$$

$$d_l^t = \left(d_{l,1}^t, \ldots, d_{l,2}^t, d_{l,p}^t\right),$$

$$d_{l,m} = K_m^l d,$$

where d is the N_s vector which indicates an output node and K_m^l is denoted by (9). $S_{k,m}$ shows the spectral density value at the mth discretized point for the kth noise source. Here, the spectral density value is independent of frequency, since only thermal noise and shot noise are treated.

If the noise signal is a stationary process, for example, flicker noise, the spectral density may have frequency dependency. In such a case, $B_{k,l}$ is used instead of $B_{k,n,l,q}$:

$$B_{k,l} = S_k(\omega).$$

It is efficient to use the adjoint method [34] for computing (34) because circuits have many noise sources. The adjoint vector X^a is defined by

$$T^t X_l^a = d_l. \tag{36}$$

Then, we have

$$\phi_{k,l,n,q} = (X_l^{at} V_k)(X_q^{a*} V_k) B_{k,l,n,q}. \tag{37}$$

A flow chart of the algorithm is shown in Fig. 3. The algorithm stops when the ratio of $\phi_{k,l,n,q}$ to ϕ_k becomes sufficiently small. The numbers L and N may be specified by the user; else they are limited by (32). Because the numerical integration time step h_m is usually sufficiently small, the limits L and N are very large. Thus, the algorithm stops before these limits are encountered in most cases. However, if $\phi_{k,N,L}/\phi_k$ is large and is not negligible, T in (16) needs to be recomputed with a smaller integration time step. The algorithms have been implemented in the circuit simulator SPREAD.

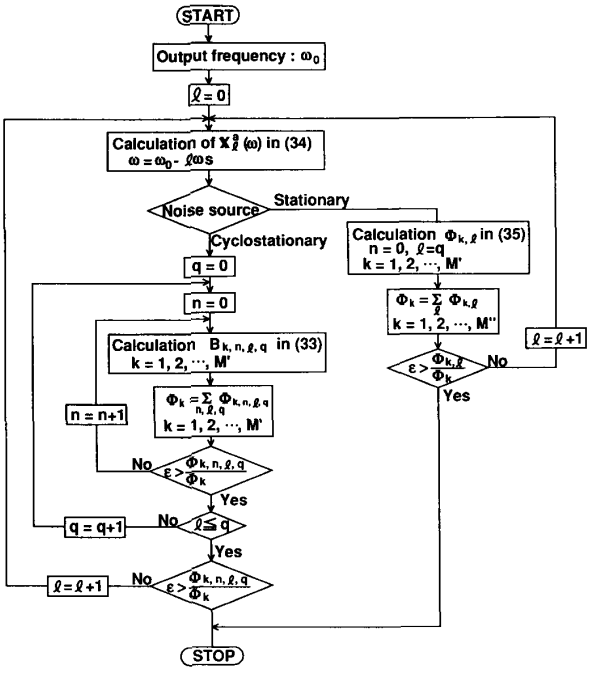

Fig. 3. Flow chart of the noise algorithm. M' = number of cyclostationary noise sources; M'' = number of stationary noise sources.

E. Comparison with an Exact Solution

The exact thermal noise of a linear resistor in a simple switching circuit was calculated and then compared with the simulation result. The power spectral density for an LPTV circuit was calculated from the Fourier transform of the time-averaged autocorrelation function [27].

As an example, consider the circuit shown in Fig. 4. The current source in Fig. 4 is an equivalent current source for the thermal noise of resistor R. The switches and the buffer in this circuit were assumed to be ideal. Using the method described in [12], the exact noise power spectral density of this circuit for a clock excitation with 50% duty cycle is calculated to be

$$\Phi_y(\omega) = \frac{k\Theta}{C} T \,\mathrm{Sa}^2\left(\frac{T\omega}{2}\right),$$

where k is the Boltzmanns constant, Θ is the absolute temperature (in kelvin), and T is the period of clock excitation. The exact solution and the simulation result are compared in Fig. 5 and are seen to match closely.

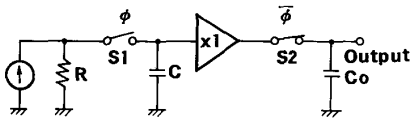

Fig. 4. S/H circuit.

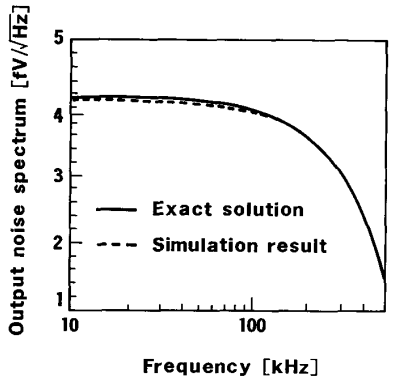

Fig. 5. Exact solution and simulation result.

IV. Examples

A. Direct Conversion Mixer Circuit

The first example was a direct conversion mixer circuit, shown in Fig. 6. The local oscillator (LO) signal frequency was 281 MHz with an RF signal at 281 MHz plus several kilohertz and gave a converted IF output signal at several kilohertz. It is exceptionally difficult to solve the steady-state response of this circuit by conventional transient analysis because of the large difference between the output frequency and the RF and LO signal frequencies. Table II(a) shows the simulation results and the measured values of the conversion gain. The operational amplifier used was LT1007CNB. The RF signal level was -50 dB (1 mW) when measured. These values matched closely when the LO signal level was low. The CPU time was 35 s for computing the periodic steady-state response with only the LO signal and was 0.8 s for computing the small signal response per RF input frequency on a SPARC/STATION2.

Table II(b) shows the simulation results and the measured values of the output noise spectrum. The shot noise of the BJT in the presence of the LO signal was modeled as cyclostationary noise. Each number of L and N in (31) has the same number of 14. When all noise sources were considered as stationary noises, the output noise spectrum was 222 nV/$\sqrt{\text{Hz}}$. The calculation result using the proposed algorithm and measured value was matched closely. Furthermore, it was found that dominant noises were thermal noises for the base resistors of $Q1$ and $Q2$ and shot noise for the base current of $Q1$.

B. Second-Order Low-Pass Filter

The second example was a second-order low-pass filter, shown in Fig. 7. The output spectrum (V_{out}) was measured

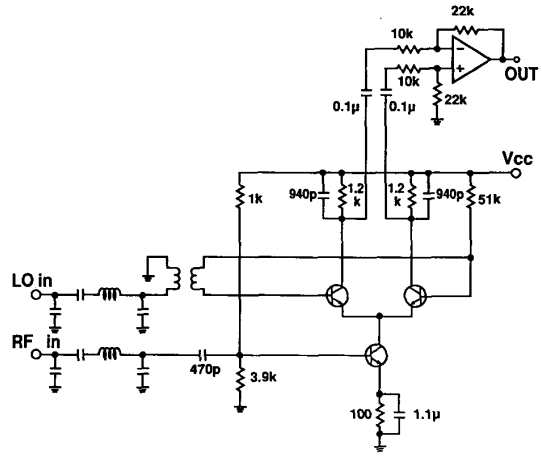

Fig. 6. Direct conversion circuit.

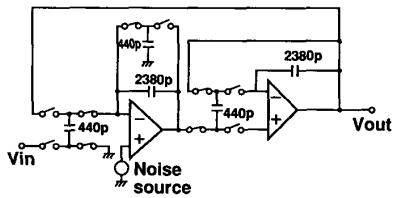

Fig. 7. Second-order low-pass filter.

TABLE II
(a) Conversion gain of the direct conversion mixer circuit

LO level [dB (1 mW)]	Measured (dB)	Simulation (dB)
−25	23.81	23.36
−20	25.48	26.73
−15	30.27	30.91
−10	30.79	31.61
−5	32.63	32.91
0	30.77	33.54

(b) Output noise spectrum of the direct conversion mixer circuit

LO level [dB (1 mW)]	Measured (nV/$\sqrt{\text{Hz}}$)	Simulation (nV/$\sqrt{\text{Hz}}$)
−20	490	516

with a fairly large input white noise source (0.25 mV/$\sqrt{\text{Hz}}$ with a 100-kHz bandwidth) inserted as shown into the first operational amplifier, to avoid uncertain internal noise contributions of the amplifiers and to increase the measurement reliability. The operational amplifiers and the switches used were CA082 and TC4016BP, respectively. The operational amplifiers were assumed to be noiseless and the switches were modeled by linear time-varying conductors with 4.7-kΩ ON resistance in the simulation; thus, the large white noise was dominant in the noise simulation. The number L in (33) was 7 for the simula-

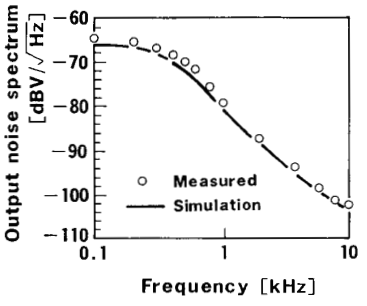

Fig. 8. Output noise spectrum of second-order low-pass filter.

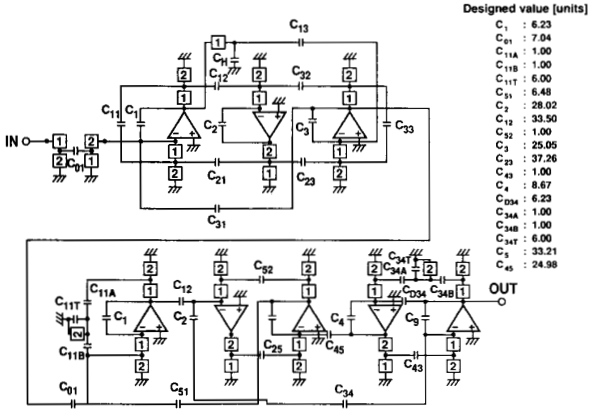

Fig. 9. Eighth-order band-pass filter.

tion. Comparison between the simulated result and the measured value of the discrete circuit is shown in Fig. 8. The simulated result matched the measured value within 2 dB.

C. Eighth-Order Band-Pass Filter

The third example was an eighth-order band-pass filter shown in Fig. 9. This circuit was made by cascading a third-order elliptic low-pass filter with a cutoff frequency of 3.4 kHz and a fifth-order elliptic high-pass filter with a cutoff frequency of 300 Hz. The sampling frequency was 100 kHz and a nominal ON resistance was 30 kΩ. The unit capacitor size was 0.2 pF with a maximum capacitor ratio of 33.5. In the simulation, linear time-varying conductances were used as switches. These switch noise sources were modeled as cyclostationary random processes. Voltage controlled voltage sources were used for the operational amplifiers.

The small signal responses of this circuit have been reported in [22]. The output noise spectrum is shown in Fig. 10. The input noise of the operational amplifier was modeled only by $1/f$ noise, which was 70 $nV/\sqrt{Hz}$ at 1 kHz using a built-in SPICE MOSFET noise model. The circles indicate measured values of IC and the solid line indicates the simulation result which matched to within 2 dB.

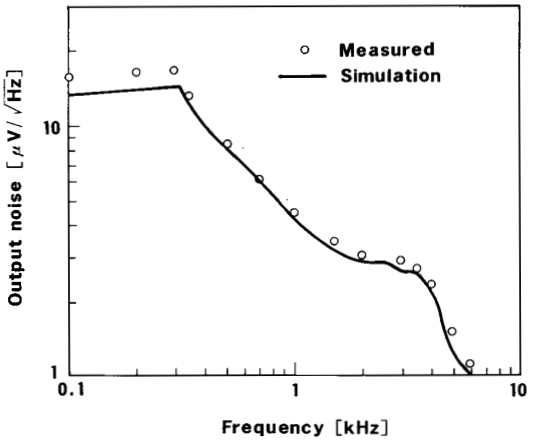

Fig. 10. Output noises of the eighth-order band-pass filter.

The CPU time for computing the periodic steady-state response with just the clock signal was 77 s, and for the complete noise analysis of this circuit was 1086 s/point on a SPARC/STATION2. The computational cost of noise analysis is still high for large-scale circuits, because all aliasing components need to be computed. However, it is expected that this problem can be greatly alleviated using a vectorization technique, because most of the computational power is used to solve linear problems.

V. Conclusions

A numerical noise analysis method for nonlinear circuits with a periodic large signal excitation has been proposed. For a small signal input response, a nonlinear circuit is modeled as a linear periodic time-varying circuit. The calculation methods for small signal characteristics and the noise figure for the linear periodic time-varying circuit have been described. The cyclostationary noise signal has been modeled by a set of independent stationary random signals with different power spectral density values. The examples showed that the simulation results and the measured values matched closely. Circuit designers can estimate the noise figures in the early stages of design, though the computational cost is still high for large scale circuits. It is further necessary to discuss the correspondence between the actual physical phenomena of noises and this modeling for cyclostationary random processes.

Acknowledgments

The authors wish to acknowledge the very helpful comments and suggestions provided by the reviewers. They would like to thank Dr. T. Shima, Y. Kamatani, A. Yasuda, C. Takahashi, T. Yamaji, and M. H. Wakayama of the Toshiba R & D Center for their valuable advice. They are also grateful to M. Hayashibara of the Communication Systems and Technology Lab., Toshiba Corp., for providing measured data.

REFERENCES

[1] L. O. Chua and A. Ushida, "Algorithm for computing almost periodic steady state response of nonlinear systems to multiple input frequencies," *IEEE Trans. Circuits Syst.*, vol. CAS-28, pp. 953–971, Oct. 1981.

[2] A. Ushida and L. O. Chua, "Frequency domain analysis of nonlinear circuits driven by multi-tone signals," *IEEE Trans. Circuits Syst.*, vol. CAS-31, pp. 766–779, Sept. 1984.

[3] A. Ushida, L. O. Chua, and T. Sugawara, "A substitution algorithm for solving nonlinear circuits with multi-frequency components," *Int. J. Circuit Thoery Appl.*, vol. 15, pp. 327–355, 1987.

[4] A. Ushida, L. O. Chua, "Steady-state response of non-linear circuit: A frequency-domain relaxation method," *Int. J. Circuit Theory Appl.*, vol. 17, pp. 249–269, July 1989.

[5] K. Kundert, J. White, and A. Sangiovanni-Vincentelli, "A mixed frequency-time approach for distortion analysis of switching filter circuits," *IEEE J. Solid-State Circuits*, vol. SC-24, no. 2, pp. 443–451, April 1989.

[6] T. J. Aprille, Jr., and T. N. Trick, "Steady-state analysis of nonlinear circuits with periodic inputs," *Proc. IEEE*, vol. 60, pp. 108–114, Jan. 1972.

[7] M. Kakizaki and T. Sugawara, "A modified Newton method for the steady-state analysis," *IEEE Trans.* Computer-Aided Design, vol. CAD-4, no. 4, pp. 662–667, Oct. 1985.

[8] K. S. Kundert and A. Sangiovanni-Vincentelli, "Simulation of nonlinear circuits in the frequency domain," *IEEE Trans. Computer-Aided Design*, vol. CAD-5, pp. 521–535, Oct. 1986.

[9] V. Rizzoli, C. Cecchetti, and A. Lipparini, "Frequency conversion in general nonlinear multiport devices," *IEEE MTT-S Int.*, pp. 483–486, June 1986.

[10] M. Kakizaki and T. Sugawara, "An efficient numerical analysis method for small signal frequency response from periodically operating circuits," *Proc. ISCAS*, pp. 579–582, 1985.

[11] W. A. Gardner, *Introduction to Random Processes*, 2nd ed. New York: McGraw-Hill, 1989, chap. 12.

[12] B. Furrer and W. Guggenbuhl, "Noise analysis of sampled-data circuits," *Proc. IEEE ISCAS*, pp. 860–863, 1981.

[13] C.-A. Gobet and A. Knob, "Noise analysis of switched capacitor network," *Proc. IEEE ISCAS*, pp. 856–859, 1981.

[14] M. L. Liou and Y.-L. Kuo, "Exact analysis of switched capacitor circuits with arbitrary inputs," *IEEE Trans. Circuits Syst.*, vol. CAS-26, no. 4, pp. 213–223, Apr. 1979.

[15] J. H. Fischer, "Noise sources and calculation techniques for switched capacitor filters," *IEEE J. Solid-State Circuits*, vol. SC-17, pp. 742–752, Aug. 1982.

[16] J. Rabaey, J. Vandewalle, and H. De Man, "A general and efficient noise analysis technique for switched capacitor filters," *Proc. IEEE ISCAS*, pp. 570–573, 1983.

[17] J. Goette and C.-A. Gobet, "Exact noise analysis of SC circuits and an approximate computer implementation," *IEEE Trans. Circuits Syst.*, vol. 36, no. 4, pp. 508–521, Apr. 1989.

[18] L. Toth and K. Suyama, "Exact noise analysis of 'ideal' SC networks," *Proc. IEEE ISCAS*, pp. 1585–1588, 1991.

[19] M. Okumura, H. Tanimoto, and T. Sugawara, "Noise analysis algorithm for periodic time-varying circuits," *Proc. IEEE ISCAS*, pp. 2173–2176, 1990.

[20] M. Okumura, T. Sugawara, and H. Tanimoto, "Noise analysis method for nonlinear circuits with two frequency excitations using the computer," *Trans. IEICE Japan*, vol. J73-A, No. 8, pp. 1342–1349, Aug. 1990 (in Japanese). Also, see *Electronics and Communications in Japan, Part 3*, vol. 74, no. 4, pp. 41–50, 1991.

[21] L. A. Zadeh, "Frequency analysis of variable networks," *Proc. IRE*, vol. 32, pp. 291–299, 1950.

[22] M. Okumura, T. Sugawara, and H. Tanimoto, "An efficient small signal frequency analysis method for nonlinear circuits with two frequency excitations," *IEEE Trans. Computer-Aided Design*, vol. CAD-9, no. 3, pp. 225–235, March 1990.

[23] L. W. Nagel, "SPICE2: A computer program to simulate semiconductor circuits," Memo. No. ERL-M520, Univ. of California, Berkeley, 1975.

[24] L. A. Zadeh and C. A. Desoer, *Linear System Theory*. New York: McGraw-Hill, 1963, chap. 6.

[25] L. O. Chua and P. M. Lin, *Computer-Aided Analysis of Electronic Circuits*. Englewood Cliffs, NJ: Prentice-Hall, Inc., 1975, chap. 12.

[26] D. Middleton, *An Introduction to Statistical Communication Theory*. New York: McGraw-Hill, 1960, chap. 11.

[27] A. Papoulis, *Probability, Random Variables, and Stochastic Processes*, 2nd ed. New York: McGraw-Hill, 1984, chap. 9.

[28] H. Ogura, "Spectral representation of a periodic nonstationary random process," *IEEE Trans. Inform. Theory*, vol. IT-17, no. 2, pp. 143–149, March 1971.

[29] W. A. Gardner and L. E. Franks, "Characterization of cyclostationary random signal processes," *IEEE Trans. Inform. Theory*, vol. IT-21, no. 1, pp. 4–14, Jan. 1975.

[30] R. A. Boyles and W. A. Gardner, "Cycloergodic properties of discrete-parameter nonstationary stochastic processes," *IEEE Trans. Inform. Theory*, vol. IT-29, no. 1, pp. 105–114, Jan. 1983.

[31] W. A. Gardner, "Rice's representation for cyclostationary processes," *IEEE Trans. Commun.*, vol. COM-35, no. 1, pp. 74–78, Jan. 1987.

[32] S. O. Rice, "Mathematical analysis of random noise," *Bell Syst. Tech. J.*, vol. 23, sec. 1.7, July 1944.

[33] M. S. Keshner, "$1/f$ noise", *Proc. IEEE*, vol. 70, no. 3, pp. 212–218, March 1982.

[34] J. Vlach and K. Singhal, *Computer Methods for Circuit Analysis and Design*. New York: Van Nostrand Reinhold, 1983, pp. 171–207.

Makiko Okumura (formerly Makiko Kakizaki) received her B.E. degree in electrical engineering from Keio University in 1982. In 1982, she joined the Toshiba Research and Development Center, Kawasaki, Japan. Since then, she has been working on the development of analog circuit simulators. She is a member of the Institute of Electronics, Information and Communication Engineers of Japan.

Hiroshi Tanimoto received his B.S., M.S., and Ph.D. degrees in elecgrical engineering from Hokkaido University, in 1975, 1977, and 1980, respectively. He joined the Toshiba Research and Development Center, Kawasaki, Japan, in 1980. His main research interests are in linear integrated circuits and analog signal processing. He is a member of the Institute of Electronics, Information and Communication Engineers and the Institute of Electrical Engineers of Japan.

Tetsuro Itakura received his B.E. degree in electronic engineering from Tokyo University of Agriculture and Technology in 1981, and his M.S. degree in electrical engineering from Stanford University, Stanford, CA, in 1989. In 1981, he joined Toshiba Corporation, Kawasaki, Japan. In recent years, he has been involved in the development of LCD driver IC's. His current interests are in signal processing and analog MOS circuits.

Tsutomu Sugawara received his B.S. and M.S. degrees in electrical engineering from Yamagata University, in 1972 and 1974, respectively. Since then, he has been with the Toshiba Research and Development Center, Kawasaki, Japan. From October 1984 to March 1986, he was a visiting scholar at the Department of Electrical Engineering and Computer Sciences, University of California, Berkeley. His research activities include the development of wireless communication systems, integrated circuits for communication systems, and their CAD systems. He is a member of the Institute of Electronics, Information and Communication Engineers of Japan and a member of IEEE.